



Effects of interstitial cluster mobility on dislocation loops evolution under irradiation of austenitic steel

Xin-Hua Yan¹ · Lu Sun¹ · Du Zhou² · Teng Xie¹ · Chang Peng¹ · Ye-Xin Yang¹ · Li Chen¹ · Zhen-Feng Tong¹

Received: 7 November 2023 / Revised: 18 December 2023 / Accepted: 9 January 2024 / Published online: 21 July 2024

© The Author(s), under exclusive licence to China Science Publishing & Media Ltd. (Science Press), Shanghai Institute of Applied Physics, the Chinese Academy of Sciences, Chinese Nuclear Society 2024

Abstract

The evolution of dislocation loops in austenitic steels irradiated with Fe⁺ is investigated using cluster dynamics (CD) simulations by developing a CD model. The CD predictions are compared with experimental results in the literature. The number density and average diameter of the dislocation loops obtained from the CD simulations are in good agreement with the experimental data obtained from transmission electron microscopy (TEM) observations of Fe⁺-irradiated Solution Annealed 304, Cold Worked 316, and HR3 austenitic steels in the literature. The CD simulation results demonstrate that the diffusion of in-cascade interstitial clusters plays a major role in the dislocation loop density and dislocation loop growth; in particular, for the HR3 austenitic steel, the CD model has verified the effect of temperature on the density and size of the dislocation loops.

Keywords Cluster dynamics · Dislocation loops · In-cascade interstitial clusters · Austenitic steels

1 Introduction

The pressurized water reactor fuel assembly support structure comprises the austenitic stainless steels Solution Annealed 304 (SA 304 SS), Cold Worked 316 (CW 316 SS), and HR3 [1, 2]. The performance degradation of these engineered alloys is primarily due to the production of various defects and defect clusters introduced by neutron irradiation, in which dislocation loops are a key factor affecting their mechanical properties [3, 4]. Because the evolution of their macroscopic properties is related to the evolution of the microstructure, understanding its evolution under irradiation is essential for predicting the time of life of internals [2]. It is

well known that simulating long-term microstructural evolution in systems involving dislocation loops currently relies on the CD model, which is one of the most popular models for dealing with irradiated microstructure evolution such as dislocation loops [2, 4–7].

Etienne used the CD model to quantitatively simulate the evolution of dislocation loops in 304 and 316 series stainless steels irradiated with Fe⁺ [2]. Although the simulation results were consistent with the experimental results, the agreement between the two sets of data was not excellent. Etienne suggested that the lack of consideration of the mobility of small point-defect clusters in the constructed CD model may be one of the reasons for the non-excellent agreement between the experimental and simulation results. According to atomistic simulations [8] and in-situ TEM observations [1, 9–11] of the mobility of irradiation-induced in-cascade clustering, small clusters (self-interstitial clusters) form directly from the irradiation cascades. The mobility of small self-interstitial clusters must be considered in the cluster dynamics model. The influence of austenitic steel interstitial cluster mobility on the evolution of dislocation loops under neutron and proton irradiation is discussed in Refs. [12] and [13]. These results demonstrate that it is reasonable to consider the mobility of interstitial clusters in the CD model.

This work was supported by the National Natural Science Foundation of China (No. U1967212), the Fundamental Research Funds for the Central Universities (No. 2021MS032), and the Nuclear Materials Innovation Foundation (No. WDZC-2023-AW-0305).

✉ Zhen-Feng Tong
tony_tzf@163.com

¹ North China Electric Power University, Beijing 102206, China

² China Nuclear Power Operations Co., Ltd, Shenzhen 518000, China

Indeed, the irradiation and material parameters as well as the reaction mechanisms considered in the model have a key impact on the accuracy of CD simulations. The irradiation parameters include the displacement rate, irradiation dose, irradiation temperature, cascade efficiency, and in-cascade clustering directly formed by the cascade [14–16]. Subsequently, CD simulates the microstructure evolution in different materials with different values of material parameters, which plays a major role in the agreement between the CD simulation results and experimental values [5]. Material parameters such as the formation energies, point defect binding energies, and migration energies of defect clusters can be obtained by ab initio calculations, molecular dynamics calculations, or experimentally [17–19]. The irradiation and material parameters are decisive input parameters in the CD model. The reaction mechanism related to defect evolution must be properly considered in the CD model, and the mobility of small self-interstitial clusters can be considered part of the reaction mechanism.

Considering the selection of input parameters and introduction of the mobility of small self-interstitial clusters in detail, the cluster dynamics model in this study predicts the evolution of dislocation loops in austenitic steel under Fe⁺ irradiation. The CD model and the solution method are described in detail in Section 2. Discussions regarding the model validation and evolution mechanisms of the dislocation loops are presented in Sect. 3. Finally, a summary of this study is presented in Sect. 4.

2 Model descriptions

2.1 Governing equations of point defects and defect clusters

The general concept and approach of CD have been described in detail and validated in the literature [4–6, 12, 13]. The main considerations and important assumptions made in the current modeling framework are as follows:

- (1) Mobile species include point defects such as self-interstitial atoms (SIA) and vacancies; small self-interstitial clusters contain two, three, and four SIAs. Only point defects can be emitted from clusters.
- (2) Formation of small defect clusters (vacancy and interstitial clusters) directly from collision cascades.
- (3) All mobile species exhibit 3D diffusion.
- (4) For mobile interstitial clusters, the migration energy is constant and independent of their size.
- (5) The pre-exponential factor of the diffusion coefficient of the interstitial clusters is the fitting parameter, which

varies with the irradiation temperature and size of the interstitial clusters.

- (6) Grain boundaries, dislocation lines, and surfaces are intrinsic sinks for mobile species.

The first four hypotheses in this model are based on the CD model described in detail in Refs. [12] and [13]. As stated in reference [13], the diffusion coefficient of interstitial clusters is calculated by the method in Ref. [18], the diffusion pre-exponential factor D_{n0} decreases monotonically with cluster size n according to the power law $D_{n0} = D_0 n^{-\delta}$. Ab initio research in Ref. [20] shows that as the temperature gradually increases from 200 to 1600 K, the pre-exponential factor of the diffusion coefficient of Fe atoms in the fcc structure Ni–Fe alloy also increases. Therefore, we assume that the parameter S decreases with increasing temperature, such that the pre-exponential factor of the diffusion coefficient of small self-interstitial clusters also increases with increasing temperature; this is qualitatively consistent with the conclusion in Ref. [20]. The irradiation temperature reported in Ref. [1] are 300 °C and 400 °C, while the temperature in Ref. [2] is 350 °C. When the temperature is 300 °C, $S = 4.5$, which is consistent with the value used in Ref. [13]. When the temperature is increased to 350 °C and 400 °C, S is taken to be 4.3 and 4.0, respectively, through the conclusion in Ref. [20] and by fitting the calculated results with the experimental results. Grain boundary and dislocation lines are intrinsic sinks that capture mobile species [21]. A surface sink is added to the model to account for the surface effects of ion irradiation. For the sake of description, the vacancies and SIA are denoted by V and I , respectively, and small self-interstitial clusters containing two, three, and four SIAs are labeled as I_2 , I_3 , and I_4 , respectively. In addition, n denotes the number of point defects in a defect cluster.

Based on the above assumptions, a series of governing equations are constructed to describe the evolution of dislocation loops. The governing equations in this model for SIA and vacancy point defects are structured as follows:

$$\begin{aligned} \frac{dC_I}{dt} = & G_{\text{irra}}^I + 2g_{I_2}^I C_{I_2} + \sum_{n=1,2,3} k_{V_n}^{I_{n+1}} C_{V_n} C_{I_{n+1}} \\ & + \sum_{n=3}^N g_{I_n}^I C_{I_n} - k_I^V C_I C_V - 2k_I^I C_I C_I - \sum_{n=2}^N k_{I_n}^I C_{I_n} C_I \\ & - \sum_{n=2}^N k_{V_n}^I C_{V_n} C_I - K_d^I D_I (C_I - C_I^{\text{eq}}) \\ & - K_{\text{gb}}^I D_I (C_I - C_I^{\text{eq}}) - K_{\text{sl}}^I D_I (C_I - C_I^{\text{eq}}) \end{aligned} \tag{1}$$

$$\begin{aligned} \frac{dC_V}{dt} = & G_{\text{irra}}^V + 2g_{V_2}^V C_{V_2} - k_I^V C_I C_V + \sum_{n=3}^N g_{V_n}^V C_{V_n} \\ & - \sum_{n=2}^N k_{I_n}^V C_{I_n} C_V - 2k_V^V C_V C_V - \sum_{n=2}^N k_{V_n}^V C_{V_n} C_V \\ & + \sum_{n=1,2,3,4} k_{V_{(n+1)}}^{I_n} C_{I_n} C_{V_{(n+1)}} - K_d^V D_V (C_V - C_V^{\text{eq}}) \\ & - K_{\text{gb}}^V D_V (C_V - C_V^{\text{eq}}) - K_{\text{sf}}^V D_V (C_V - C_V^{\text{eq}}) \end{aligned} \tag{2}$$

The form of the governing equations describing the change in the concentrations of interstitial clusters I_n ($n = 2, 3, 4$) and vacancy clusters V_n ($n = 2, 3, 4$) is

$$\begin{aligned} \frac{dC_{I_n}}{dt} = & G_{\text{irra}}^{I_n} - g_{I_n}^I C_{I_n} + g_{I_{n+1}}^I C_{I_{n+1}} - K_{\text{sf}}^{I_n} D_{I_n} C_{I_n} \\ & + \sum_{m=1, m+n \leq 4} k_{V_m}^{I_{m+n}} C_{I_{m+n}} C_{V_m} - \sum_{m=1}^N k_{V_m}^{I_n} C_{V_m} C_{I_n} \\ & + \sum_{m=1, 2m \leq n} k_{I_m}^{I_{n-m}} C_{I_m} C_{I_{n-m}} - K_d^{I_n} D_{I_n} C_{I_n} \\ & - K_{\text{gb}}^{I_n} D_{I_n} C_{I_n} - \left(\sum_{m=1}^N k_{I_m}^{I_n} C_{I_m} C_{I_n} + k_{I_n}^{I_n} C_{I_n} C_{I_n} \right) \end{aligned} \tag{3}$$

$$\begin{aligned} \frac{dC_{V_n}}{dt} = & G_{\text{irra}}^{V_n} - g_{V_n}^V C_{V_n} + g_{V_{n+1}}^V C_{V_{n+1}} - k_{V_n}^V C_{V_n} C_V \\ & + k_{V_{n-1}}^V C_{V_{n-1}} C_V - \sum_{m=1}^4 k_{V_n}^{I_m} C_{V_n} C_{I_m} \\ & + \sum_{m=1}^4 k_{V_{m+n}}^{I_m} C_{V_{m+n}} C_{I_m} \end{aligned} \tag{4}$$

Disregarding the irradiation cascade generation term $G_{\text{irra}}^{V_n}$ in Eq. (4), a general form of the governing equations for vacancy clusters with sizes greater than four can be obtained. The governing equation for immobile dislocation loops with a size greater than four is as follows:

$$\begin{aligned} \frac{dC_{I_n}}{dt} = & \sum_{m=1, 2m \leq n} k_{I_m}^{I_{n-m}} C_{I_m} C_{I_{n-m}} - \sum_{m=1}^4 k_{I_n}^{I_m} C_{I_n} C_{I_m} \\ & + k_{I_{n+1}}^V C_{I_{n+1}} C_V - k_{I_n}^V C_{I_n} C_V + g_{I_{n+1}}^I C_{I_{n+1}} - g_{I_n}^I C_{I_n} \end{aligned} \tag{5}$$

Specifically, C_I and C_V are the concentrations of SIA and vacancy point defects, respectively, whereas C_I^{eq} and C_V^{eq} are the thermal equilibrium concentrations of SIA and vacancies, respectively. The density of interstitial clusters/loops comprising n SIAs is denoted by C_{I_n} , and that of vacancy clusters is denoted by C_{V_n} . The thermal equilibrium concentrations of the dislocation loops $C_{I_n}^{\text{eq}}$ ($n \geq 2$) and vacancy clusters $C_{V_n}^{\text{eq}}$ ($n \geq 2$) are zero, $G_{\text{irra}}^{I_n}$ and $G_{\text{irra}}^{V_n}$ are generation rates of small self-interstitial clusters ($n \leq 4$) and

small vacancy clusters ($n \leq 4$), respectively, directly from intra-cascade clustering [2, 6, 22]. $k_{I_n}^\theta$ and $k_{V_n}^\theta$ are the rate coefficients of the dislocation loops and vacancy clusters of size n , respectively, that absorb mobile defect θ . Dislocation loops and vacancy clusters can emit only SIAs and vacancy point defects, respectively. $g_{I_n}^I$ is the rate at which dislocation loops emit SIA, and $g_{V_n}^V$ is the rate at which vacancy clusters emit vacancies. D_I and D_V are the diffusion coefficients of the SIAs and vacancies, respectively, with D_{I_n} being the diffusion coefficient of the mobility interstitial clusters. K_d^θ , K_{gb}^θ and K_{sf}^θ are the sink strengths of dislocation lines, grain boundary, and surfaces, respectively. The formalisms of the rate coefficient and sink strength etc. is discussed in detail in Sect. 2.2.

The model described in Sect. 2.1 corresponds to Model-4 in this study, which represents an mobile interstitial cluster with a maximum size of four. In this study, to analyze the influence of mobile interstitial clusters on the density and size of dislocation loops predicted by the CD model, we construct three types of cluster dynamics models: those in which only a single SIA can move, those in which at most two interstitial clusters can move, and those in which interstitial clusters of size three can move; these cluster dynamics models correspond to Model-1, Model-2, and Model-3, respectively. For vacancy clusters, Model-1 to Model-4 assume that only vacancies can move. The input parameters, such as the irradiation and material parameters, are the same for Model-1 to Model-4, as shown in Tables 1 and 2 in Sect. 2.4. The capture of mobile defects by dislocation lines, grain boundaries, and surface sinks has been considered in the four models. The main difference between the models is the size of the maximum mobile interstitial cluster. As the maximum mobile interstitial cluster gradually increases, the generation and disappearance terms required in the governing equations describing the evolution of defects of a certain

Table 1 Irradiation parameters used in CD model for different irradiation conditions

Symbol	Value
Temperature, T (°C)	300, 350, 400 [1, 2]
Dose rate, G_{dpa} (dpa/s)	2.9×10^{-4} [1, 2] 2.2×10^{-3}
Cascade efficiency, η	0.15 [6]
Di-interstitial fraction in cascade, f_{I_2}	0.5 [6]
Tri-interstitial fraction in cascade, f_{I_3}	0.2 [6]
Four-interstitial fraction in cascade, f_{I_4}	0.2 [6]
Di-vacancy fraction in cascade, f_{V_2}	0.05 [6]
Tri-vacancy fraction in cascade, f_{V_3}	0.05 [6]
Four-vacancy fraction in cascade, f_{V_4}	0.02 [6]

Table 2 Material parameters for CW 316, SA 304 and HR3 stainless steels

Symbol	Value
Lattice parameter, a_0 (nm)	0.363 [27]
Burgers vector, b	$a_0/\sqrt{2}$ [28]
Vacancy formation energy, E_f^V (eV)	1.7 [2]
Interstitial formation energy, E_f^{SIA} (eV)	4.1 [2]
Pre-exponential factor, D_0 (cm^2s^{-1})	10^{-3} [2]
Power-law exponent, S	4.5, 4.3*, 4.0* [13]
Vacancy migration energy, E_m^V (eV)	1.3 [29]
Interstitial migration energy, E_m^{SIA} (eV)	0.45 [2]
Di-interstitial binding energy, $E_{I_2}^b$ (eV)	0.61 [2]
Di-vacancy binding energy, $E_{V_2}^b$ (eV)	0.45 [6]
Dislocation density, ρ_{dis} (cm^{-2})	10^6 [2] 10^{10}
Average grain size, d_{gb} (μm)	40 [6]
Thickness of the thin foil, $2d$ (nm)	100 [2]

The symbol * indicates that S is the fitting parameter, and the default indicates the value used in Ref. [13]

size in different models change accordingly. All models assume that mobile defects undergo 3D diffusion; that is, the rates of mutual reactions between defects are calculated according to the 3D-3D expression. For brevity, Sect. 2 only introduces the construction of Model-4 in detail; the other three models are similar to Model-4.

2.2 Rate coefficients

The generation rates of defects from the in-cascade are taken from Ref. [6] which considered the formation of clusters with sizes greater than four unlikely. The defect-generation terms are as follows:

$$\begin{aligned}
 G_{\text{irra}}^I &= \eta G_{\text{dpa}} (1 - f_{I_2} - f_{I_3} - f_{I_4}) \\
 G_{\text{irra}}^{I_n} &= \frac{\eta G_{\text{dpa}} f_{I_n}}{n} \quad (n \leq 4) \\
 G_{\text{irra}}^V &= \eta G_{\text{dpa}} (1 - f_{V_2} - f_{V_3} - f_{V_4}) \\
 G_{\text{irra}}^{V_n} &= \frac{\eta G_{\text{dpa}} f_{V_n}}{n} \quad (n \leq 4)
 \end{aligned} \tag{6}$$

G_{dpa} denotes the damage rate under irradiation and η is the cascade efficiency. f_{I_n} and f_{V_n} are the generation fractions of interstitial clusters and vacancy clusters of size n that survive the reorganization events following the cascade, respectively.

k_I^V is the characteristic annihilation rate of the SIA and vacancy point defects, which can be expressed as:

$$k_I^V = 4\pi r_{IV} (D_I + D_V) \tag{7}$$

where r_{IV} is the recombination radius.

By adopting the formalism in Ref. [23], the rate coefficients of dislocation loops and vacancy clusters that absorb mobile defects are:

$$k_{I_n}^\theta = 2\pi (D_{I_n} + D_\theta) (r_{I_n} + r_\theta) Z_{I_n}^\theta \quad (\theta = I, V), \tag{8}$$

$$k_{V_n}^\theta = 4\pi (D_V + D_\theta) (r_{V_n} + r_\theta) \quad (\theta = I, V). \tag{9}$$

In Eq. (8), $Z_{I_n}^\theta$ is the bias factor of the dislocation loops, which can be calculated using the method described in Ref. [5]. In particular, the diffusion coefficient D_{I_n} is calculated using the method described in Ref. [18]:

$$D_{I_n} = D_0 n^{-s} \exp\left(-\frac{E_m^I}{k_B T}\right) \quad (n \leq 4) \tag{10}$$

The rate coefficients for the emission of point defect SIAs and vacancies by dislocation loops and vacancy clusters are Ref. [24]

$$g_{I_n}^I = \frac{k_{I_{n-1}}^I}{V_{\text{at}}} \exp\left(-\frac{E_{I_n}^b}{k_B T}\right) \tag{11}$$

$$g_{V_n}^V = \frac{k_{V_{n-1}}^V}{V_{\text{at}}} \exp\left(-\frac{E_{V_n}^b}{k_B T}\right) \tag{12}$$

The binding energies $E_{I_n}^b$ and $E_{V_n}^b$ in Eqs. (11) and (12) can be determined using the following extrapolation law [25]

$$E_{I_n}^b = E_I^f + \frac{E_{I_2}^b - E_I^f}{2^{\frac{2}{3}} - 1} (n^{2/3} - (n-1)^{2/3}) \tag{13}$$

$$E_{V_n}^b = E_V^f + \frac{E_{V_2}^b - E_V^f}{2^{\frac{2}{3}} - 1} (n^{2/3} - (n-1)^{2/3}) \tag{14}$$

where E_I^f and E_V^f are the formation energies of the SIAs and vacancies, respectively. $E_{I_2}^b$ and $E_{V_2}^b$ are the binding energies for the interstitial and vacancy clusters of size two, respectively.

The sink strength of dislocation lines is

$$K_d^\theta = Z_D^\theta \rho_{\text{dis}} \quad (\theta = I, V) \tag{15}$$

where Z_D^θ is the bias for the dislocation lines absorbing SIA or vacancies. $Z_D^I = 1.1$ and $Z_D^V = 1.0$ are adopted from Ref. [6]. ρ_{dis} is the density of the dislocation lines, assuming that the density of dislocation lines ρ_{dis} remains unchanged during irradiation.

The expressions for the sink strengths of the grain boundary and surfaces were adopted in Ref. [26]. They can be given as:

$$K_{gb}^\theta = \frac{6\sqrt{S_m^\theta}}{d_{gb}} \quad (\theta = I, V) \tag{16}$$

$$K_s^\theta = \frac{\sqrt{S_m^\theta}}{d} \frac{1}{\coth\left(\sqrt{S_m^\theta}d\right) - \frac{1}{\sqrt{S_m^\theta}d}} \quad (\theta = I, V) \tag{17}$$

where d_{gb} is the grain size and d is the half thickness of the thin foil. S_m^θ represents the total sink strength of the medium without surfaces. Similar to Ref. [4], the bias of the dislocation loops to the interstitial clusters I_2, I_3 and I_4 is $Z_{I_n}^{I_2} = Z_{I_n}^{I_3} = Z_{I_n}^{I_4} = Z_{I_n}^I$, the bias of the dislocation lines to the interstitial clusters I_2, I_3 and I_4 is $Z_D^{I_2} = Z_D^{I_3} = Z_D^{I_4} = Z_D^I$, the sink strength of the grain boundary and surface to the interstitial clusters I_2, I_3 and I_4 are $k_{gb}^{I_2} = k_{gb}^{I_3} = k_{gb}^{I_4} = k_{gb}^I$ and $k_{sf}^{I_2} = k_{sf}^{I_3} = k_{sf}^{I_4} = k_{sf}^I$.

The coupled equation, Eqs. (1)–(5), along with the input parameters detailed in Sect. 2.4, are considered in the evolution system of dislocation loops involving the largest interstitial clusters $I_{(n=117000)}$. Thousands of equations must be solved by using this system, which requires a significant amount of simulation time. The Grouping method [30] and the Fokker–Planck method [4–6] have been used to reduce the number of equations to be solved in the system to reduce the simulation time. Parallel-solution methods reduce the simulation time of the system [31]. In this study, the discrete rate equations are transformed into Fokker–Planck equations to improve simulation efficiency. Its specific form is described in Sect. 2.3.

2.3 Fokker–Planck method

The dislocation loop evolution system described by the CD model contains a large number of ordinary differential equations (ODEs), which need to be solved. One of the main reasons for the increase in the simulation time of the cluster dynamics is the number of ODEs in the model; the more equations there are, the longer the CD simulation requires. In addition, the stiffness of the equations is also a major factor that increases the time and complexity of solving CD models. The simulation efficiency can be improved by reducing the number of equations in the system and selecting an appropriate ODE solver. The Fokker–Planck (F–P) method has been applied to reduce the number of ordinary differential equations in cluster dynamics models [4–6, 27, 32]. When the F–P method is applied, the part of the dislocation loop evolution system described by the discrete rate equations is called the discrete part, and the part that transforms the discrete rate equation into the F–P equation

through Taylor expansion is the continuous part [32]. In this study, we assume that the interstitial and vacancy clusters in the discrete part range from $I_{n=1}$ to $I_{n=100}$ and $V_{n=1}$ to $V_{n=100}$, when $n > 100$; that is, the equations within the continuous part, Eqs. (4) and (5) can be transformed into F–P equations as follows:

$$\frac{\partial C(x, t)}{\partial t} = -\frac{\partial}{\partial x} \left\{ F(x, t)C(x, t) - \frac{\partial}{\partial x} [D(x, t)C(x, t)] \right\} \tag{18}$$

where $F(x, t)$ is the drift term related to the growth in cluster size x . $D(x, t)$ is the diffusion term related to the nucleation of clusters [32].

For interstitial clusters, the drift term $F_I(x, t)$ and the diffusion term $D_I(x, t)$.

$$F_I(x, t) = \sum_{m=1,2,3,4} mk_x^m C_{I_m} - g_x^I - k_x^V C_V \tag{19}$$

$$D_I(x, t) = \frac{1}{2} \left[\sum_{m=1,2,3,4} m^2 k_x^m C_{I_m} + g_x^I + k_x^V C_V \right] \tag{20}$$

For vacancy clusters,

$$F_V(x, t) = k_{V_x}^V C_{V_x} C_V - \sum_{m=1,2,3,4} mk_{V_x}^m C_{V_x} C_{I_m} - g_{V_x}^V \tag{21}$$

$$D_V(x, t) = \frac{1}{2} \left[\sum_{m=1,2,3,4} m^2 k_{V_x}^m C_{I_m} + g_{V_x}^V + k_{V_x}^V C_V \right] \tag{22}$$

Equation (18) can be discretized into the following form by using the central difference method [33]

$$\begin{aligned} \frac{\partial C(x_i, t)}{\partial t} = & \frac{2}{\Delta x_{i+1} + \Delta x_i} \left[\frac{1}{2} (F(x_{i-1}, t)C(x_{i-1}, t) - F(x_{i+1}, t)C(x_{i+1}, t)) \right. \\ & \left(\frac{D(x_{i+1}, t)C(x_{i+1}, t) - D(x_i, t)C(x_i, t)}{\Delta x_{i+1}} \right. \\ & \left. \left. - \frac{D(x_i, t)C(x_i, t) - D(x_{i-1}, t)C(x_{i-1}, t)}{\Delta x_i} \right) \right] \end{aligned} \tag{23}$$

In Eq. (23), subscript i is the index of the divided grid point, the dislocation loop size at index i is denoted x_i , and the relationship between the dislocation loop size at index i and the dislocation loop size at index $i + 1$ is $x_{(i+1)} = x_i + \Delta x_i$, where Δx_i is the step size of the grid at index i . To reduce the number of equations, it is necessary to divide the nonuniform grid, that is, $\Delta x_i = 1.01\Delta x_{(i-1)}$. Using the F–P method, the number of F–P equations describing the evolution of the dislocation loop density in the continuous part is 750, and the number of F–P equations describing the evolution of the vacancy cluster density in the continuous part is 900. Combined with the number of discrete rate equations, only 1850 equations must be solved in the system to describe the

evolution of dislocation loops with a maximum radius of 42 nm. The accurate discrete rate equations require hundreds of thousands of equations to describe the evolution of dislocation loops; therefore, the F–P method significantly reduces the number of equations in the system and improves the efficiency of the solution. The numerical solution of this dislocation loops evolution system is calculated using the Fortran wrappers of ODEPACK algorithms, the ODE solver such as CVODE in which is suitable for solving stiffness problems [34].

2.4 Input parameters

The HR3 austenitic stainless steel was irradiated with Fe⁺ in Ref. [1] The SA304 and CW316 stainless steels were irradiated with Fe⁺ in Ref. [2]. The irradiation and material parameters from the two studies can be used as input parameters for the CD model in this study, as shown in Tables 1 and 2.

3 Results and discussion

3.1 Effect of mobile interstitial clusters on dislocation loops evolution

Suppose that the size of the largest mobile interstitial cluster in the CD model gradually increases from one to four, corresponding to Model-1, Model-2, Model-3 and Model-4 respectively. Figure 1 shows the dislocation loop size distribution simulated by the four models at a dose of 0.145 dpa under the same irradiation conditions.

The ordinate in Fig. 1 is the logarithm of the dislocation loop density; therefore, the lowest density of dislocation loops cannot be considered as zero. In this study, we use $C_{\text{loop}} = 10 \times 10^{-11} \text{ cm}^{-3} \approx 0 \text{ cm}^{-3}$ for the plot. However, in the CD model, similar to [4], we set the number of evolution

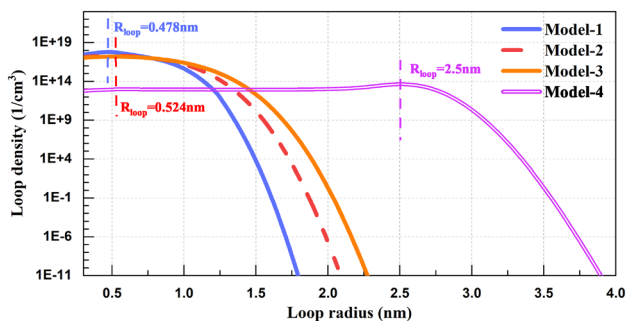


Fig. 1 (Color online) Dislocation loops size distribution simulated by Model-1 to Model-4, and modeling at $G_{\text{dpa}} = 2.9 \times 10^{-4}$ dpa/s, $t = 500$ s, $T = 350$ °C

equations describing the dislocation loops and vacancy clusters sufficiently large to ensure that the integral value describing the maximum defect cluster in the system is zero. The blue, red dotted, orange, and purple curves shown in Fig. 1 show the dislocation loop size distribution curves predicted by Model-1, Model-2, Model-3 and Model-4, respectively. The blue vertical dashed line indicates the dislocation loops radius $R_{\text{loop}} = 0.478$ nm corresponding to the peak dislocation loops density predicted by Model-1; Model-2 and Model-3 predicted dislocation loops peak densities corresponding to the same radius $R_{\text{loop}} = 0.524$ nm. The dislocation loops radius corresponding to the dislocation loops peak densities predicted by Model-2 and Model-3 is marked with an orange vertical dashed line. The purple vertical dashed line marks the dislocation loop size $R_{\text{loop}} = 2.5$ nm corresponding to the peak dislocation loop density predicted by Model-4. Figure 1 shows that under the same irradiation conditions, when the dislocation loops average radius $R_{\text{loop}} < 0.478$ nm, Model-1 predicts that the dislocation loops density gradually increases, and when $R_{\text{loop}} = 0.478$ nm, the dislocation loops density reaches the peak $C_{\text{loop}}^{\text{peak}} = 5.9 \times 10^{17} \text{ cm}^{-3}$, when the dislocation loops density predicted by Model-1 is zero, $R_{\text{loop}} = 1.8$ nm, the total number density of dislocation loops predicted by Model-1 is $C_{\text{loop}} = 1.3 \times 10^{19} \text{ cm}^{-3}$. When the dislocation loop radius $R_{\text{loop}} < 0.524$ nm, the dislocation loop density predicted by Model-2 and Model-3 increases slowly, and the dislocation loop density reaches the peak values of $C_{\text{loop}}^{\text{peak}} = 2.09 \times 10^{17} \text{ cm}^{-3}$ and $C_{\text{loop}}^{\text{peak}} = 1.57 \times 10^{17} \text{ cm}^{-3}$, respectively, at $R_{\text{loop}} = 0.524$ nm. When the predicted value of the dislocation loops density of Model-2 is zero, $R_{\text{loop}} = 2.1$ nm, and when the predicted value of the dislocation loops density of Model-3 is zero, $R_{\text{loop}} = 2.25$ nm. The total densities of dislocation loops predicted by Model-2 and Model-3 are $C_{\text{loop}} = 7.22 \times 10^{18} \text{ cm}^{-3}$ and $C_{\text{loop}} = 6.43 \times 10^{18} \text{ cm}^{-3}$. In the prediction of Model-4, when $R_{\text{loop}} < 2.5$ nm, the dislocation loop density continues to increase. At $R_{\text{loop}} = 2.5$ nm, the dislocation loop density reaches the peak value $C_{\text{loop}}^{\text{peak}} = 4.28 \times 10^{13} \text{ cm}^{-3}$. At $R_{\text{loop}} = 3.9$ nm, the dislocation loop density is zero. Model-4 predicts that the number density of dislocation loops is $C_{\text{loop}} = 3.22 \times 10^{15} \text{ cm}^{-3}$. A comparison of the simulation results of the four models is shown in Fig. 1; this comparison shows that, under the same irradiation conditions, as the mobile interstitial cluster gradually increases from SIA to interstitial cluster I_4 , the peak $C_{\text{loop}}^{\text{peak}}$ of the dislocation loop density and the number of dislocation loop densities predicted by Models-1 to Models-4 start to decrease, and the radius corresponding to the peak dislocation loop density increases. By comparing the radius corresponding to a dislocation loop density of zero, we can see that the distribution of the dislocation loop size predicted by Model-1 to Model-4 becomes wider and trending towards a larger size.

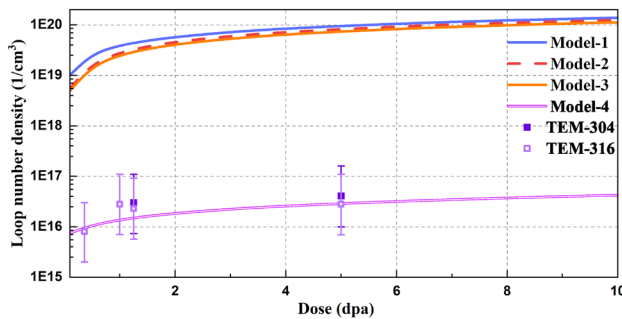


Fig. 2 (Color online) Comparison of the average loop number density at 10 dpa simulated by Model-1 to Model-4 with the experimental data in [2]. Modeling at $G_{\text{dpa}} = 2.9 \times 10^{-4}$ dpa/s, $T = 350$ °C

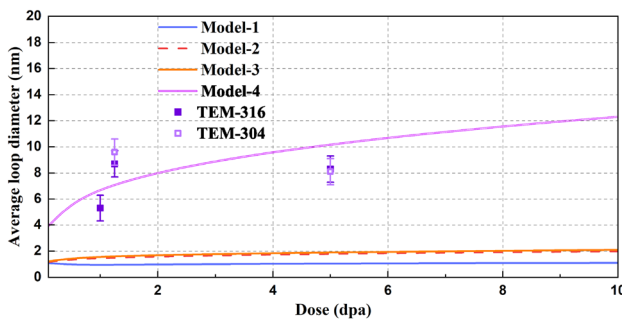


Fig. 3 (Color online) Comparison of the average loop diameter at 10 dpa simulated by Model-1 to Model-4 with the experimental data in [2]. Modeling at $G_{\text{dpa}} = 2.9 \times 10^{-4}$ dpa/s, $T = 350$ °C

The curves in Figs. 2 and 3 show a comparison of the number density and the average diameter of the dislocation loops when the four models are simulated to 10 dpa, respectively. The scatter values are the TEM observations of the number density and average diameter of the dislocation loops, respectively, in Ref. [2].

Model-1 in Fig. 2 predicts a blue curve corresponding to the highest dislocation loop density. The dislocation loop densities predicted by Model-2 and Model-3 are indicated by red dashed and orange curves, respectively. Figure 2 shows that the dislocation loop densities predicted by Model-2 and Model-3 are almost identical, with a very small difference. In fact, the dislocation loop density predicted by Model-2 is higher than that predicted by Model-3. Compared with the other three models, Model-4 predicts the lowest dislocation loop density. In general, with an increase in the largest mobile interstitial cluster size, the number density of the dislocation loops simulated from Model-1 to Model-4 decreases. With an increase in the radiation dose, the dislocation loop density predicted by the four models gradually increased, and the growth rate of the dislocation loop density decreased; that is, the dislocation loop density tended to saturate with the increase in the dose.

In contrast to Fig. 2, compared with the other three models, the average diameter of dislocation loops predicted by Model-4 in Fig. 3 is the highest, whereas that predicted by Model-1 is the lowest. Similar to Fig. 2, the average diameters of the dislocation loops predicted by Model-3 and Model-2 were almost the same, but the average diameter of the dislocation loops predicted by Model-3 was larger than that predicted by Model-2. Therefore, in Fig. 3, the average diameter of the dislocation loops simulated from Model-1 to Model-4 increased with the increasing cluster size of the largest mobile interstitial cluster. As the irradiation dose increased, the average diameter of the dislocation loops simulated by Model-1 to Model-3 tended to stabilize after 1 dpa, with almost no growth. However, the average diameter of the dislocation loops predicted by Model-4 still has a high growth rate after 1 dpa, and does not tend to saturate even at 10 dpa; the predicted value of Model-4 is also much larger than the predicted values of the other three models.

The simulation results shown in Figs. 1, 2 and 3 can be attributed to three reasons: on the one hand, the dislocation loop number density obtained by Model-4 in Fig. 2 is the smallest; however, the average diameter of the dislocation loops obtained using Model-4 in Fig. 3 is the largest. In addition, the dislocation loop size distribution simulated by Model-1 to Model-4 in Fig. 1 evolves to a larger size at 0.145 dpa. These results indicate that increasing the size of mobile interstitial clusters can promote dislocation loop growth. In fact, the molecular dynamics simulation in Ref. [8] demonstrates that interstitial clusters can move, and the experiment in Ref. [1] demonstrates that interstitial clusters can migrate and merge to promote dislocation loop growth. Therefore, the increase in the size of the mobile interstitial clusters may be the main reason for the increase in the size of the dislocation loops simulated in Model-4. Second, with the increase in the size of mobile interstitial clusters, they are captured by dislocation loops, vacancy clusters, surfaces, grain boundaries, and dislocation line sinks, which can explain the density of dislocation loops obtained from Model-1 to Model-4 in Fig. 2 decreases with an increase in the size of the mobile interstitial clusters. Third, because the largest in-cascade interstitial cluster in the CD model is less than three, an in-cascade interstitial cluster greater than three is still generated; however, an in-cascade interstitial cluster greater than three can't be diffused and migrated. These non-migratory clusters themselves produce an accumulation, resulting in an increase in the density of dislocation loops, and also serve as a sink for mobile interstitial clusters, thus inhibiting the growth of dislocation loops to a large size distribution. This explains the reasons that lead to the almost less than 2.25 nm radius distribution of dislocation loops predicted by

Model-1 to Model-3 in Fig. 1 and the average diameter of the dislocation loops predicted by Model-1 to Model-3 in Fig. 3, which consistently approximates 2 nm.

The density and average diameter of the dislocation loops in SA304 and CW316 steels irradiated by Fe^+ ions observed by TEM in Ref. [2] are compared with the simulation data of Model-1 to Model-4. The experimental results agree well with the simulation results of Model-4. The reasons for the better simulation results of Model-4 may be summarized in two points. First, the fraction of in-cascade interstitial clusters obtained in Ref. [22] shows that there are few in-cascade interstitial clusters with a size greater than four; therefore, it is reasonable to assume that the maximum mobile interstitial cluster size is four. In addition, as mentioned previously, the mobility of the interstitial clusters in the model may be the main reason why the simulation results of Model-4 are in good agreement with the experimental results. The experimental results agree well with the simulation results of Model-4, indicating that it is reasonable to consider the mobility of the interstitial clusters in the CD model.

3.2 Effect of temperature on mobile interstitial clusters

In this section, the CD model(Model-4) constructed in this study is used to simulate the evolution of dislocation loops in HR3 steel, as observed during in-situ electron microscopy in Ref. [1]. Figures 4 and 5 show comparisons between the CD predictions and the experimental data for the number density and average diameter of dislocation loops at 300 °C and 400 °C, respectively.

The experimental values of the number density and average diameter of the dislocation loops shown in Figs. 4 and 5 are affected by both the irradiation temperature and irradiation dose. The experimental values in Fig. 4 demonstrate that, as the temperature increases, the number

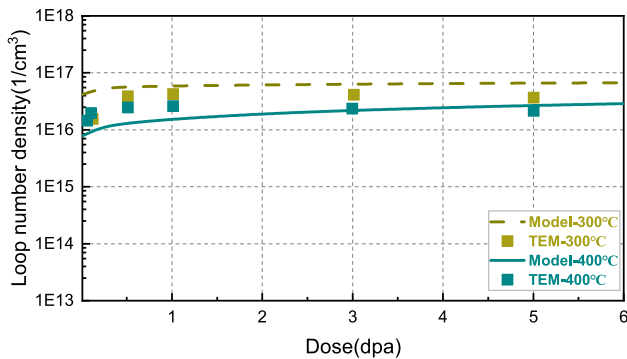


Fig. 4 (Color online) Comparison of the loop number density at 6 dpa simulated by CD with the experimental data in Ref. [1] at different temperatures

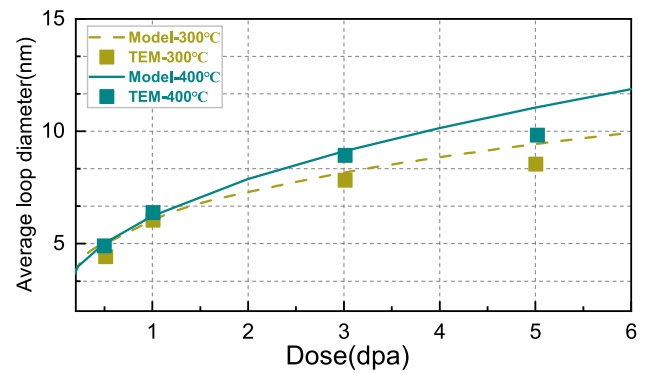


Fig. 5 (Color online) Comparison of the average loop diameter at 6 dpa simulated by CD with the experimental data in Ref. [1] at different temperatures

density of dislocation loops decreases. This is because high temperatures promote the growth and aggregation of dislocation loops, while limiting the nucleation of new dislocation loops [1]. As mentioned in the model description, the pre-exponential factor of the diffusion coefficient of mobile interstitial clusters in this paper varies with the size of mobile interstitial clusters n and temperature T . Based on this hypothesis, $T = 300$ °C, $S = 4.5$, $T = 400$ °C, $S = 4.0$. With the increase in temperature, the value of S decreases and the pre-exponential factor of the diffusion coefficient of interstitial clusters increases; thus, the diffusivity of interstitial clusters increases. Enhancing the diffusion ability of interstitial clusters can promote the migration and accumulation of dislocation loops.

The CD model in Fig. 4 predicts the number density of dislocation loops under irradiation conditions of 300 °C and 400 °C, respectively. With increasing temperature, the predictions of the CD model remain consistent with the experimental data. Similarly, the average diameters of the dislocation loops simulated using the CD model, as shown in Fig. 5, are in good agreement with the experimental data, and the average diameter of the dislocation loops increases with increasing temperature.

As shown in Fig. 4, the experimental value of the dislocation loop density reaches saturation at 0.5 dpa and begin to decrease with increasing radiation doses. Reference [1] assumed that the increase of irradiation dose promotes the merging of dislocation loops and formation of network dislocations, which limits the increase in the number density of dislocation loops during irradiation. Stoller constructed an evolution model of network dislocation under irradiation, which means that the variation in network dislocation density due to the possible growth and unfaulting of dislocation loops, activation of Bardeen-Herring sources, and irradiation-enhanced climb of dislocations have been considered in Ref. [35]. The CD model in this study does not consider the network dislocation evolution, i.e., the

density of network dislocations is constant. Therefore, as the irradiation dose increases, the CD model predicts that the number density of dislocation loops slowly increases and tends to saturate. This trend differs slightly from that of the experimental data for the number density of dislocation loops. In addition, the CD predictions of the average diameters of the dislocation loops still tend to grow toward larger sizes. The dislocation loop number density is slightly larger than the experimental values shown in Fig. 4 for CD simulations up to 5 dpa and 6 dpa; this may have contributed to the larger average diameter of the dislocation loops in Fig. 5 for CD predictions with irradiation doses of up to 5 dpa. Adding a network dislocation evolution mechanism to the CD model should be considered in future studies.

4 Conclusion

In this study, considering the mobility of interstitial clusters and selecting appropriate input parameters, a cluster dynamics model was constructed to simulate the number density and average size of dislocation loops in SA304, CW316, and HR3 austenitic steels irradiated using Fe⁺ ions. The main conclusions are summarized as follows:

- (1) The simulation results from Model-1 to Model-4 show that as the size of the mobile interstitial cluster increases in the CD model, the dislocation loop density decreases and the dislocation loop size increases. The simulation results of Model-4 were more consistent with the experimental results in the literature. This demonstrates that it is reasonable to consider the diffusion mechanism of the interstitial clusters in the CD model.
- (2) The CD simulation results of the average diameter and number density of the dislocation loops are in good agreement with the results of in-situ ion irradiation in the literature, which accurately reflects the effect of temperature on the density and size of the dislocation loops: that is, as the temperature increases, the density of the dislocation loops decreases, and the size of the dislocation loops increases.
- (3) The mechanism of network dislocation evolution under irradiation is not considered in the CD model, which may be the main reason for the slight inconsistency between the simulation results of the CD model and the experimental data. Adding a network dislocation evolution mechanism to the CD model should be considered in future studies.

Author Contributions All authors contributed to the study conception and design. Material preparation, data collection and analysis were

performed by Xin-Hua Yan, Lu Sun and Zhen-Feng Tong. The first draft of the manuscript was written by Xin-Hua Yan and all authors commented on previous versions of the manuscript. All authors read and approved the final manuscript.

Data availability The data that support the findings of this study are openly available in Science Data Bank at <https://cstr.cn/31253.11.sciencedb.j00186.00079> and <https://www.doi.org/10.57760/sciencedb.j00186.00079>.

Declarations

Conflict of interest The authors declare that they have no Conflict of interest.

References

1. J.P. Wang, L. Guo, J.R. Luo et al., In-situ TEM investigation of dislocation loop evolution in HR3 steel during Fe⁺ ion irradiation. *J. Nucl. Mater.* **578**, 154309 (2023). <https://doi.org/10.1016/j.jnucmat.2023.154309>
2. A. Etienne, M. Hernández-Mayoral, C. Genevois et al., Dislocation loop evolution under ion irradiation in austenitic stainless steels. *J. Nucl. Mater.* **400**, 56–63 (2010). <https://doi.org/10.1016/j.jnucmat.2010.02.009>
3. P. Jin, T.L. Shen, J. Li et al., Spherical nanoindentation stress-strain responses of SIMP steel to synergistic effects of irradiation by H and He ions. *Nucl. Sci. Tech.* **33**, 79 (2022). <https://doi.org/10.1007/s41365-022-01053-7>
4. C. Chen, Y.X. Wei, L.P. Guo et al., Rate theory study of the proton-irradiation induced dislocation loops in modified 310S steels. *Nucl. Instrum. Meth. B.* **461**, 181–185 (2019). <https://doi.org/10.1016/j.nimb.2019.09.028>
5. A.H. Duparc, C. Moingeon, N. Smetniansky-de-Grande et al., Microstructure modelling of ferritic alloys under high flux 1 MeV electron irradiations. *J. Nucl. Mater.* **302**, 143–155 (2002). [https://doi.org/10.1016/S0022-3115\(02\)00776-6](https://doi.org/10.1016/S0022-3115(02)00776-6)
6. C. Pokor, Y. Brechet, P. Dubuisson et al., Irradiation damage in 304 and 316 stainless steels: experimental investigation and modeling. Part I: Evolution of the microstructure. *J. Nucl. Mater.* **326**, 19–29 (2004). <https://doi.org/10.1016/j.jnucmat.2003.11.007>
7. F. Li, C. Chen, D.X. Guo et al., Rate theory and experimental study of the irradiation induced defects in molybdenum alloy. *J. Alloys Compd.* **874**, 159751 (2021). <https://doi.org/10.1016/j.jallcom.2021.159751>
8. D. Terentyev, N. Castin, Mobility of small clusters of self-interstitial atoms in dilute Fe-Cr alloy studied by means of atomistic calculations. *Comp. Mater. Sci.* **46**, 1178–1186 (2009). <https://doi.org/10.1016/j.commatsci.2009.06.004>
9. Y. Luo, Y. Dong, X. Wang et al., In-situ TEM study of the effect of pre-existing dislocation on loop evolution in 508-III steel during Fe⁺ irradiation. *J. Nucl. Mater.* **559**, 153420 (2022). <https://doi.org/10.1016/j.jnucmat.2021.153420>
10. X.Y. Chen, A.L. Wen, C.L. Ren et al., Theoretical prediction of radiation-enhanced diffusion behavior in nickel under self-ion irradiation. *Nucl. Sci. Tech.* **31**, 79 (2020). <https://doi.org/10.1007/s41365-020-00791-w>
11. G. Yang, Y.K. Wu, Y.F. Ding et al., Effect of ion flux on one-dimensional migration of dislocation loops in Fe₉Cr_{1.5}W_{0.4}Si F/M steel during in-situ Fe⁺ irradiation. *J. Nucl. Mater.* **579**, 154412 (2023). <https://doi.org/10.1016/j.jnucmat.2023.154412>
12. J. Gan, G.S. Was, R.E. Stoller, Modeling of microstructure evolution in austenitic stainless steels irradiated under light water

- reactor condition. *J. Nucl. Mater.* **299**, 53–67 (2001). [https://doi.org/10.1016/S0022-3115\(01\)00673-0](https://doi.org/10.1016/S0022-3115(01)00673-0)
13. Y. Abe, S. Jitsukawa, N. Okubo et al., in *Effects of Radiation on Nuclear Materials*, vol. 25, ed. by T. Yamamoto (ASTM International, West Conshohocken, 2013), p. 313
 14. S. Wu, H. Cao, J.D. Wang et al., Cascades damage in γ -iron from molecular dynamics simulations. *Mater. Sci. Forum.* **993**, 1011–1016 (2020). <https://doi.org/10.4028/www.scientific.net/MSF.993.1011>
 15. W.J. Xiao, G.Y. Wu, M.H. Li et al., MD and OKMC simulations of the displacement cascades in nickel. *Nucl. Sci. Tech.* **27**, 57 (2016). <https://doi.org/10.1007/s41365-016-0057-y>
 16. G.Y. Wu, N.W. Hu, H.Q. Deng et al., Simulation of radiation damages in molybdenum by combining molecular dynamics and OKMC. *Nucl. Sci. Tech.* **28**, 3 (2017). <https://doi.org/10.1007/s41365-016-0164-9>
 17. W. Xiao, X. Zhang, W.T. Geng et al., Helium bubble nucleation and growth in α -Fe: insights from first-principles simulations. *J. Phys. Condens. Matter.* **26**, 255401 (2014). <https://doi.org/10.1088/0953-8984/26/25/255401>
 18. Y.N. Osetsky, D.J. Bacon, A. Serra et al., Stability and mobility of defect clusters and dislocation loops in metals. *J. Nucl. Mater.* **276**, 65–77 (2000). [https://doi.org/10.1016/S0022-3115\(99\)00170-1](https://doi.org/10.1016/S0022-3115(99)00170-1)
 19. H.E. Schaefer, K. Maier, M. Weller, D. Herlach, A. Seeger, J. Diehl, Vacancy formation in iron investigated by positron annihilation in thermal equilibrium. *Scr. Metall.* **11**, 803–809 (1977). [https://doi.org/10.1016/0036-9748\(77\)90079-5](https://doi.org/10.1016/0036-9748(77)90079-5)
 20. J.D. Tucker, R. Najafabadi, T.R. Allen et al., Ab initio-based diffusion theory and tracer diffusion in Ni-Cr and Ni-Fe alloys. *J. Nucl. Mater.* **405**, 216–234 (2010). <https://doi.org/10.1016/j.jnucmat.2010.08.003>
 21. L. Guo, F. Luo, Y. Yu, *Dislocation Loops in Irradiated Nuclear Materials* (National Defense Industry Press, Beijing, 2017), pp.159–166
 22. R.E. Stoller, L.R. Greenwood, Subcascade formation in displacement cascade simulations: implications for fusion reactor materials. *J. Nucl. Mater.* **271–272**, 57–62 (1999). [https://doi.org/10.1016/S0022-3115\(98\)00730-2](https://doi.org/10.1016/S0022-3115(98)00730-2)
 23. C.J. Ortiz, P. Pichler, T. Fühner et al., A physically based model for the spatial and temporal evolution of self-interstitial agglomerates in ion-implanted silicon. *J. Appl. Phys.* **96**, 4866–4877 (2004). <https://doi.org/10.1063/1.1786678>
 24. C. Dethloff, E. Gaganidze, V.V. Svetukhin, Modeling of helium bubble nucleation and growth in neutron irradiated boron doped RAFM steels. *J. Nucl. Mater.* **426**, 287–297 (2012). <https://doi.org/10.1016/j.jnucmat.2011.12.025>
 25. J. Gao, E. Gaganidze, B. Kaiser et al., Integrated modeling of helium-vacancy clustering in Eurofer97 steel upon He⁺/Fe³⁺ + dual-beam irradiation. *J. Nucl. Mater.* **547**, 152822 (2021). <https://doi.org/10.1016/j.jnucmat.2021.152822>
 26. F. Christien, A. Barbu, Effect of self-interstitial diffusion anisotropy in electron-irradiated zirconium: a cluster dynamics modeling. *J. Nucl. Mater.* **346**, 272–281 (2005). <https://doi.org/10.1016/j.jnucmat.2005.06.024>
 27. N.M. Ghoniem, S. Sharafat, A numerical solution to the Fokker–Planck equation describing the evolution of the interstitial loop microstructure during irradiation. *J. Nucl. Mater.* **92**, 121–135 (1980). [https://doi.org/10.1016/0022-3115\(80\)90148-8](https://doi.org/10.1016/0022-3115(80)90148-8)
 28. R.E. Stoller, G.R. Odette, A composite model of microstructural evolution in austenitic stainless steel under fast neutron irradiation. Paper presented at the 13th international symposium on effects of radiation on materials. Seattle, WA, 23–25 June (1986)
 29. T. Okita, W.G. Wolfer, A critical test of the classical rate theory for void swelling. *J. Nucl. Mater.* **327**, 130–139 (2004). <https://doi.org/10.1016/j.jnucmat.2004.01.026>
 30. S.I. Golubov, A.M. Ovcharenko, A.V. Barashev et al., Grouping method for the approximate solution of a kinetic equation describing the evolution of point-defect clusters. *Philos. Mag. A.* **81**, 643–658 (2001). <https://doi.org/10.1080/01418610108212164>
 31. J.J. Li, J.L. Li, Y. Yang et al., A parallel ETD algorithm for large-scale rate theory simulation. *J. Supercomput.* **78**, 14215–14230 (2022). <https://doi.org/10.1007/s11227-022-04434-2>
 32. T. Jourdan, G. Bencteux, G. Adjanor, Efficient simulation of kinetics of radiation induced defects: a cluster dynamics approach. *J. Nucl. Mater.* **444**, 298–313 (2014). <https://doi.org/10.1016/j.jnucmat.2013.10.009>
 33. Y.G. Li, W.H. Zhou, R.H. Ning et al., A cluster dynamics model for accumulation of helium in tungsten under helium ions and neutron irradiation. *Commun. Comput. Phys.* **11**, 1547–1568 (2012). <https://doi.org/10.4208/cicp.030311.090611a>
 34. S.D. Cohen, A.C. Hindmarsh, P.F. Dubois, CVODE, a stiff/nons-tiff ODE solver in C. *Comput. Phys.* **10**, 138–143 (1996). <https://doi.org/10.1063/1.4822377>
 35. R.E. Stoller, Modeling dislocation evolution in irradiated alloys. *Metall. Trans. A* **21**, 1829–1837 (1990). <https://doi.org/10.1007/BF02647229>

Springer Nature or its licensor (e.g. a society or other partner) holds exclusive rights to this article under a publishing agreement with the author(s) or other rightsholder(s); author self-archiving of the accepted manuscript version of this article is solely governed by the terms of such publishing agreement and applicable law.